Progress In Electromagnetics Research, Vol. 105, 253–272, 2010

BANDWIDTH ENHANCEMENT OF AN ANALOG FEEDBACK AMPLIFIER BY EMPLOYING A NEGATIVE GROUP DELAY CIRCUIT

H. Choi and Y. Jeong

Division of Electronics and Information Engineering
Chonbuk National University
664-14 Deokjin-dong, Deokjin-gu, Jeonju
Chonbuk 561–756, Republic of Korea

C. D. Kim

Sewon Teletech, Inc.
881 Kwanyang, Dongahn, Anyang
Geonggi 431–804, Republic of Korea

J. S. Kenney

School of ECE
Georgia Institute of Technology
Atlanta, GA 30332, USA

Abstract—We will demonstrate an alternative topology to greatly increase the operating bandwidth of an analog RF feedback power amplifier. A limited operating bandwidth due to the group delay mismatch of a feedback loop discouraged the use of an RF feedback technique in spite of its powerful linearization performance and great tolerance capability. By introducing a negative group delay circuit (NGDC) in the feedback loop, group delay match condition could be satisfied. With the fabricated 2-stage distributed element negative group delay circuit with a 30 MHz of bandwidth and a −9 ns of group delay for a wideband code division multiple access (WCDMA) downlink band, the proposed feedback amplifier with the proposed topology experimentally achieved an adjacent channel leakage ratio of −53.2 dBc with a cancellation bandwidth of over 50 MHz.

Corresponding author: Y. Jeong (ycjeong@jbnu.ac.kr).

1. INTRODUCTION

Power amplifiers are essential components in a communication system and are inherently nonlinear. The nonlinearity generates spectral regrowth, which leads to adjacent channel interference and violations of the out-of-band emission requirements. Digital predistortion (DPD) can provide good linearity at the digital domain, but this results in very complicated algorithm, limited bandwidth, and expensive solution [1]. Since its introduction by Black [2] and the experiment by Seidel [3], the feedforward amplifier system has played a leading role in linear transmitters, especially in the base-station applications used in a modern wireless communication environment. The feedforward linearization is well known for its broad bandwidth capability, good linearization performance, and its stable operation. However, poor system efficiency is the critical disadvantage of the feedforward amplifier [4–13].

In addition to the feedforward method, Seidel also introduced a feedback amplifier [14, 15], which utilizes the main and error amplifiers with three signal coupling devices used to degenerate the error signal generated by the main amplifier by introducing a feedback loop [16–20]. McRory et al. [16] mathematically analyzed the same structure based on the Volterra series. Kim et al. [17] proposed a modified version of the feedback topology and named the circuit 'feedback predistortion'. Qiang et al. [18] also analyzed the structure introduced by Seidel based on power series expansion. There are notable advantages in the feedback amplifier when compared to the feedforward amplifier: 1) the EPA requires lower output power since the error signal is injected to the input of the MPA, and 2) the RF output loss is smaller because there is no lossy GD element at the output of the MPA. Regardless of all these advantages, an extremely narrow operating bandwidth, which is only capable of covering a few megahertz, was the key limiting factor that discouraged the utilization of the feedback topology. This is especially true in the recent wireless communication environment, which utilizes several digital modulation schemes involving modulated signals with a broad bandwidth, such as wideband code division multiple access (WCDMA) and worldwide interoperability for microwave access (WiMAX). This limited bandwidth of feedback amplifier originates from the GD mismatching generated in the feedback loop by the feedback transmission time. In the conventional researches the minimum feedback time is assumed, but in a practical situation the assumption is not valid because of the transmission time of the MPA, EPA, and other signal adjusting devices including the band-pass filter [19, 20].

Recently, some interesting studies have led to the experimental validation, and electronic circuit application of a negative group delay (NGD) or negative group velocity concept have been undertaken. The NGD concept is quite intriguing, and sometimes confusing, in that typical materials under normal conditions do not usually behave in a manner consistent with the observed behaviors. In the specific frequency band of an anomalous dispersion or signal attenuation, the group velocity is observed to be greater than c, the speed of light in vacuum, or even a negative value. This phenomenon was defined as the superluminal group velocity [21, 22]. Researchers have been trying to find applications using NGD or the superluminal effect in various electronic circuits [23–25]. In [26], a trial to design a passive negative group delay circuit (NGDC) for the feedforward power amplifier application was reported. However, due to a narrow signal bandwidth (2 MHz of 2-tone spacing), poor input/output reflection coefficients, design inaccuracies induced by the limited availability of lumped elements, and the fact that there was no intuitive general NGDC design equation, the previous work was not suitable for a commercial linear power amplifier system for broadband modulated signals, such as WCDMA signals in which the signal bandwidth is roughly 5 MHz for a single carrier signal. Considering the inter-modulation distortion (IMD) signal, the bandwidth requirements would be much harder to satisfy in practical applications. In [27–30], various applications of the NGD circuits with an active topology have been proposed. Choi et al. [31] has proposed the general design equation of lumped element design for the NGD circuit, and proposed the NGD circuit with distributed element topology for easy and precise design [32]. Jeong et al. [33] indirectly proved the time advancement property of the NGD circuit by using signal cancellation loop.

This paper presents a novel topology applied to a feedback amplifier with an enhanced bandwidth by adopting the time advancement property of the NGDC. The major benefit that can be achieved with the proposed topology is a bandwidth enhancement accomplished by providing GD matching at the feedback loop, without affecting the linearization performance.

2. THE FEEDBACK ARCHITECTURE AND ANALYSIS

2.1. The Feedforward and Feedback Amplifier

Figure 1 shows the feedforward and feedback architectures introduced by Seidel. Due to the forward loops as shown in Fig. 1(a), the feedforward structure is unconditionally stable. Fig. 1(b) shows the feedback amplifier structure. The RF output power loss is smaller

than the feedforward structure since there is no GD component at the output of the MPA_{FB}. In addition, the required power capability for the EPA is smaller in the feedback structure because the error signal is injected into the input port of the MPA, while the error signal in the feedforward structure is injected into the output port of the MPA which requires a higher power level, therefore degrading the system efficiency. Typically a band-pass filter is utilized in the feedback loop to prevent unwanted oscillation. Although in-band oscillation is suppressed by the negative feedback loop, out of band oscillation is possible when a positive feedback occurs.

According to Seidel's statement however, the error-correcting technique, known as the feedback, attempts a causal contradiction: after an event has occurred, the feedback attempts to reshape the cause. Although he assumed the event would be slow enough and the feedback action fast enough, the GD is unavoidable as long as there is a propagation time for the MPA_{FB}, the EPA_{FB} and the accompanying adjustable devices required for loop balancing. Due to the GD mismatch, the cancellation bandwidth of the feedback amplifier has been limited to a very narrow bandwidth, discouraging the use of this technique in modern broadband wireless communications. This is discussed in more detail in the following subsection.

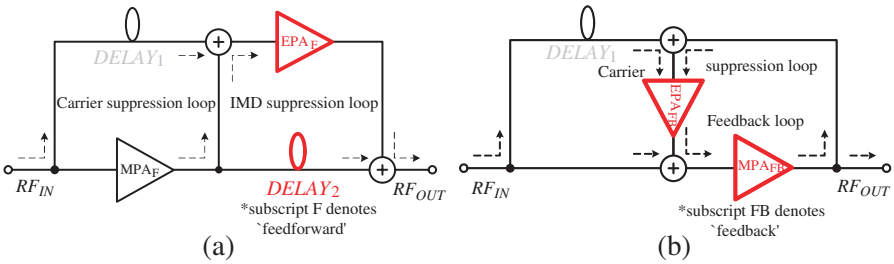

Figure 1. The comparison of the typical feedforward and feedback structures: (a) the feedforward amplifier and (b) the feedback amplifier.

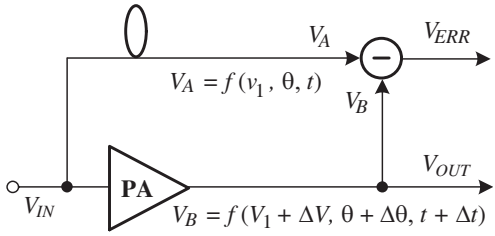

Figure 2. A simple signal suppression loop model.

2.2. Group Delay Mismatch and Bandwidth Limitation in a Feedback Structure

To understand the source of a limited cancellation bandwidth in a feedback amplifier, we need to mathematically analyze the signal cancellation loop. Fig. 2 shows a simple signal suppression loop model representing the amplitude, out-of-phase, and GD mismatches. A portion of the input signal (V_{IN}) is coupled into the delay path as a reference signal (V_A). The remaining portion of the V_{IN} is amplified by the PA resulting in an amplified carrier with IMD components. A portion of the output of the PA (V_B) is then coupled into the subtraction circuit, which is then destructively combined with the V_A, generating an error signal (V_{ERR}) that theoretically does not include any carrier components.

1) The amplitude and out-of-phase mismatch: When the reference signal of a sinusoidal waveform having an amplitude (V_1) and a phase (θ) is combined with the signal that includes the amplitude mismatch factor (ΔV) and the out-of-phase mismatch factor ($\Delta\theta$), the resultant carrier suppressed signal can be represented as a ratio of the average power of V_{ERR} to V_A [5].

$$S(\text{dB}) = 10\log\left[1 + \left(\frac{V_1 + \Delta V}{V_1}\right)^2 - 2\left(\frac{V_1 + \Delta V}{V_1}\right)\cdot\cos(\Delta\theta)\right] \quad (1)$$

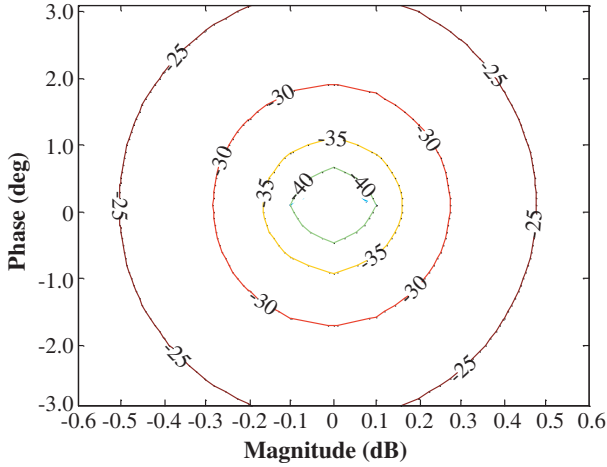

Figure 3. Loop suppression expressed as a function of the amplitude and the out-of-phase mismatch.

Figure 3 shows the calculated loop suppression performance expressed as a function of the amplitude mismatch and the out-of-phase mismatch. From the figure, mismatch range within the amplitude mismatch of ± 0.3 dB and the out-of-phase mismatch of $\pm 2^\circ$ leads to a loop suppression of about -30 dB, where the GD mismatch is assumed to be zero in this analysis.

2) The group delay mismatch: The GD mismatch (Δt) between the paths is critical for the broadband signal suppression. For our analysis, we assumed a unit amplitude ($V_1 = 1$) and a perfectly matched amplitude and out-of-phase condition ($\Delta V = \Delta\theta = 0$). V_{ERR} can be expressed as follows, where ω_0 is an angular frequency:

$$\begin{aligned} V_{ERR} &= V_A - V_B = \cos(\omega_0 t + \theta) + \cos(\omega_0(t + \Delta t) + \theta + 180^\circ) \\ &= \cos(\omega_0 t + \theta) + (1 - \cos(\omega_0 \Delta t)) + \sin(\omega_0 t + \theta)\sin(\omega_0 \Delta t) \end{aligned} \quad (2)$$

To calculate the average power over one period, $|V_{ERR}|^2$ can be obtained by using (2).

$$\begin{aligned} |V_{ERR}|^2 \;=\; & \left| \frac{(1 - \cos\omega_0\Delta t)^2 + (1 - \cos\omega_0\Delta t)^2 \cos 2(\omega_0 t + \theta)}{2} \right. \\ & + \frac{\sin^2(\omega_0\Delta t) + \sin^2(\omega_0\Delta t)\sin^2(\omega_0 t + \theta)}{2} \\ & \left. + \sin 2(\omega_0 t + \theta)(1 - \cos\omega_0\Delta t)(\sin\omega_0\Delta t) \right| \end{aligned} \quad (3)$$

By taking an integral of (3) over an arbitrary period T_0, the average power of V_{ERR} is given by (4).

$$P_{ERR,avg} = 1 - \cos\omega_0\Delta t \quad (4)$$

Since the ratio of (4) to the average power of the V_A ($P_A = 1/2$) is defined as the loop suppression, we can express the loop suppression in a dB scale for a time mismatch condition as shown in (5):

$$S_{\Delta t} = 10\log(1 - (\cos(\omega_0\Delta t)) \cdot (1 - f/f_0)) + 3 \quad (5)$$

where the term $1 - f/f_0$ is inserted to derive the equation with respect to the normalized frequency ($\text{Frequency}_{\text{norm}}$ in Fig. 4) when f_0 represents the center frequency.

Finally, from (1) and (5) we can derive the loop suppression equation considering the amplitude, out-of-phase and GD mismatches to be represented as a function of time (Δt).

$$S_{total} = 10\log\left[1 + \left(\frac{V_1 + \Delta V}{V_1}\right)^2 - 2\left(\frac{V_1 + \Delta V}{V_1}\right) \cdot \cos(\omega_0\Delta t)\left(1 - \frac{f}{f_0}\right)\right] \quad (6)$$

Figure 4 shows the loop suppression performance with and without the presence of the GD mismatch for a fixed amplitude mismatch of

0.01 dB. In the case where there is no GD mismatch, as shown in Fig. 4(a), the loop suppression performance is only limited by the out-of-phase mismatch, not by the normalized frequency, as the dotted arrow designates. However, in the presence of a GD mismatch of 0.3 ns, the amount of the loop suppression performance is limited both by the phase (solid line) and the normalized frequency (dotted line), as shown in Fig. 4(b).

Figure 5 shows the calculated and the simulated loop suppression performance, with respect to the normalized frequency, for a different GD mismatch when there is an amplitude mismatch of 0.01 dB with no out-of-phase mismatch. The mathematical estimation closely agrees with the circuit simulation obtained by using the ADS 2009 program. Fractional bandwidth variation for loop suppression of 20 dB with respect to the group delay mismatch is illustrated in Fig. 6. In case of the 0.3 ns GD mismatch, we expect that the fractional bandwidth for a 20 dB cancellation will be 5.2%. When the mismatch is 1.0 ns, the bandwidth is considerably reduced to 1.6%. The cancellation bandwidth is reduced to 30% of the bandwidth for a 0.3 ns mismatch.

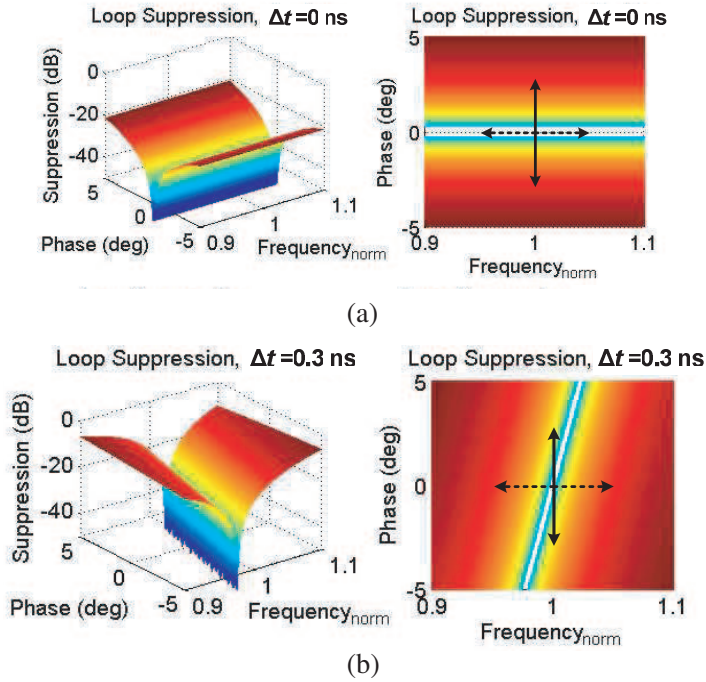

Figure 4. Loop suppression performance expressed as a function of phase and group delay mismatch when: (a) $\Delta t = 0$ ns and (b) $\Delta t = 0.3$ ns (@ fixed amplitude mismatch of 0.01 dB).

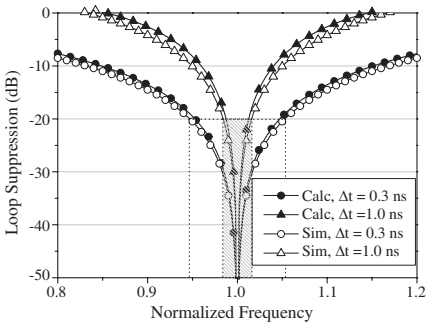

Figure 5. Calculated and simulated loop suppression performance expressed as a function of the normalized frequency for the different group delay mismatching values.

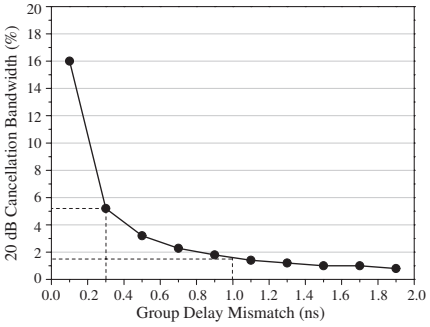

Figure 6. Calculated fractional bandwidth for loop suppression of 20 dB according to the group delay mismatch.

2.3. Analog Feedback Amplifier Employing a Negative Group Delay Circuit

Figure 7 illustrates the proposed feedback amplifier employing the NGDC, which consists of the $\mathrm{MPA_{FB}}$, the $\mathrm{EPA_{FB}}$, the vector modulators, an input coupler, an error injection coupler, the output sampling coupler, the band-pass filter, and the NGDC. In the first instance, a portion of the input signal (RF_{IN}) is applied to the $\mathrm{MPA_{FB}}$ and experiences the full gain of the amplifier. Secondly, the remaining input signal is used as a reference (A) against which a portion of the amplified output signal (B) is compared. Any difference between the reference signal and the output signal, due to noise or distortion, is identified as an error signal (C). The error signal is amplified in a separate $\mathrm{EPA_{FB}}$, and then injected (D) into the input port of the $\mathrm{MPA_{FB}}$ in phase in order to generate the error-free RF_{OUT}. The graphical representation of the test signals and nonlinear distortions shown in Fig. 7 are derived from the open loop condition. Due to the feedback path delay, which consists of the sum of the $\mathrm{MPA_{FB}}$, the output sampling coupler, the band-pass filter, the carrier cancellation circuit, and the vector modulator, plus an additional delay of π radians at the center frequency, the system bandwidth is fairly limited. By introducing the NGDC into the feedback loop between the output sampling coupler and the band-pass filter, the feedback path delay can be controlled to increase the cancellation bandwidth.

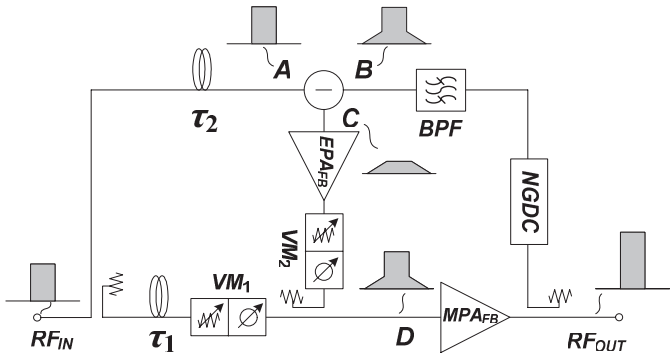

Figure 7. The block diagram of the proposed feedback amplifier.

3. CIRCUIT IMPLEMENTATION

The design equations for the transmission type series-parallel (SP) and shunt-series (SS) NGDC have already been derived in [31]. A reflective circuit, however, is useful to improve the input/output reflection characteristics of RF circuits, such as a variable phase shifter and a variable attenuator using a 3 dB hybrid [32]. Fig. 8 shows the lumped element (LE) prototype circuits for the reflective parallel (RP) and the reflective series (RS) NGDC. The magnitude and phase of the reflection coefficient (Γ_{RP}) for the RP network can be obtained by using the input impedance of the RP network. Using this, the GD and the return loss are represented by (7) and (8) by assuming a resonance condition for the desired operating frequency. The GD is a function of the capacitance (C_{RP}) and the resistance (R_{RP}).

$$GD_{RP}|_{\omega=\omega_0} = -\frac{d\varphi_{in,RP}}{d\omega}|_{\omega=\omega_0} = \frac{4R_{RP}^2 Y_0 C_{RP}}{(R_{RP}Y_0)^2 - 1} \tag{7}$$

$$\Gamma_{RP}|_{\omega=\omega_0} = \frac{1 - R_{RP}Y_0}{1 + R_{RP}Y_0} \tag{8}$$

For good understanding and design, (7) and (8) were calculated using a MATLAB program according to C_{RP} and R_{RP}, especially for $40\,\Omega < R_{RP} < 60\,\Omega$ and $0\,\text{pF} < C_{RP} < 10\,\text{pF}$ as shown in Fig. 9. The amount of NGD is proportional to R_{RP} and C_{RP}, provided that R_{RP} is smaller than $50\,\Omega$. In the case of $R_{RP} > 50\,\Omega$, the NGDC abruptly causes a positive GD. From the subplot of Fig. 9, illustrating the return loss with respect to R_{RP}, it can be inferred that more NGD induces more signal attenuation, delivering a trade-off to the designer, as the reflection coefficient is equal to the insertion loss for the reflective circuit.

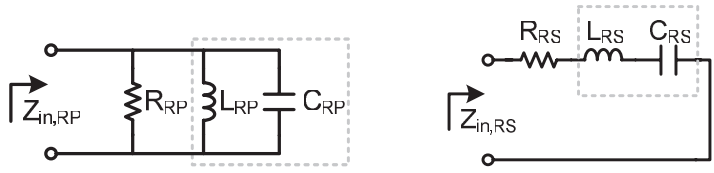

Figure 8. The lumped element prototype negative group delay circuits: (a) the reflective parallel structure and (b) the reflective series structure.

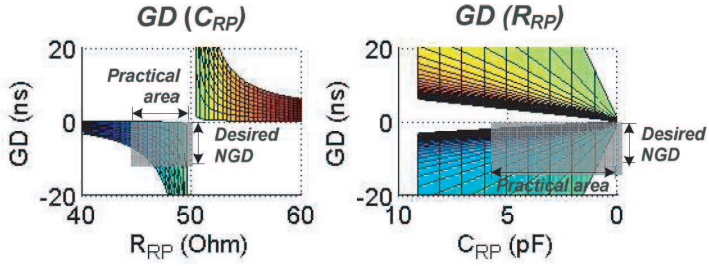

Figure 9. Calculated group delay and the return loss according to R_{RP} and C_{RP}.

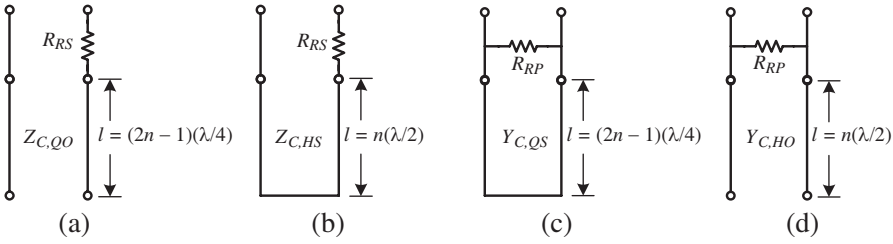

Figure 10. The four types of distributed element negative group delay circuits: (a) quarter-wavelength open, (b) half-wavelength short, (c) quarter-wavelength short, and (d) half-wavelength open, from [32].

One major difficulty found in the LE circuit is the feasibility of realizing the designed component values. In a microwave circuit design, a specific length of open or short terminated transmission line can be used as a resonator, called a transmission line resonator (TLR) [34]. Fig. 10 shows the four types of DE NGDCs converted from the LE prototype NGDCs. It is noted that Figs. 10(a) and (c) have an odd

multiple of the quarter-wavelength, and Figs. 10(b) and (d) have a multiple of the half-wavelength, with $n = 1$ being chosen to get a small size. The RP network in Fig. 8(a) can be converted either into the quarter-wavelength short circuit (QS) of Fig. 10(a) or the half-wavelength open circuit (HO) of Fig. 10(b). The RS network in Fig. 8(b) can be converted either into the quarter-wavelength open circuit (QO) of Fig. 10(c) or the half-wavelength short circuit (HS) of Fig. 10(d). The characteristic impedance and admittance for the four types of TLR can be derived as follows, respectively:

$$Y_{C,QS} = \frac{4\omega_0 C_{RP}}{\pi} \tag{9}$$

$$Y_{C,HO} = \frac{2\omega_0 C_{RP}}{\pi} \tag{10}$$

$$Z_{C,HS} = \frac{2\omega_0 L_{RS}}{\pi} \tag{11}$$

$$Z_{C,QO} = \frac{4\omega_0 L_{RS}}{\pi} \tag{12}$$

An example to show the validity of the LE prototype RP NGDC and its equivalent DE circuit were simulated. By using (7) and Fig. 9, we calculated that an $R_{RP} = 47.5\,\Omega$, a $C_{RP} = 5.0\,\text{pF}$, and an $L_{RP} = 1.107\,\text{nH}$ was necessary to achieve a NGD of $-9\,\text{ns}$. The estimated return loss was $-31.82\,\text{dB}$, derived from (8), at a center frequency of 2.14 GHz. Then, the LE circuit was converted into the TLR using (9). The calculated characteristic impedance for the QS was $60.16\,\Omega$, as shown in Fig. 10. Since there are a number of combinations for LC resonating pairs, C_{RP} should be carefully chosen so that the characteristic impedance of TLR should not exceed the practical range. Larger amount of NGD value beyond 10 ns involves the bandwidth limitation as well as the higher insertion loss. As a prototype, a microstrip 3 dB branchline coupler is designed as a 90° hybrid. To reduce the circuit size, a commercial, low profile, and miniature 3 dB hybrid coupler with the surface mount package can be used.

For experimental verification, we set as our goal the design of a 2-stage reflective DE NGDC with a total GD of $-9\,\text{ns}$, close to 0 dB insertion loss, and a 30 MHz bandwidth centered on the WCDMA downlink band ($2.125 \sim 2.155\,\text{GHz}$). This NGD value was chosen for the compensation of the signal propagation time due to the circuits in the EPA path in the feedback structure, including the band-pass filter. The proposed circuit would be constructed of 90° hybrids and two DE NGDC units (#1 and #2) in which the center frequencies were 2.125 GHz and 2.155 GHz, respectively, as shown in Fig. 11. By connecting the two units in a cascade, it was expected to obtain a

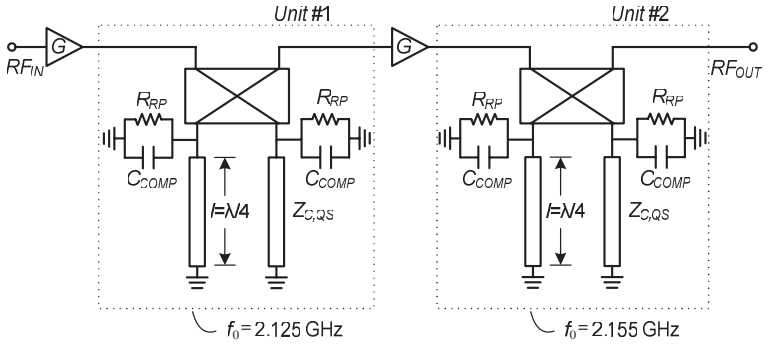

Figure 11. The circuit diagram of a 2-stage reflection type negative group delay circuit, from [32].

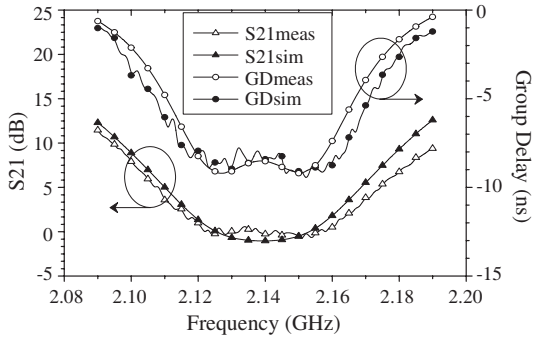

Figure 12. The simulated and measured group delays and insertion losses of the 2-stage reflection type negative group delay circuit.

flat GD and transmission response. The insertion loss of the NGDC itself could be compensated by a general purpose small signal amplifier, as shown in Fig. 11. A compensation capacitor (C_{COMP}) would be connected in parallel to R_{RP} to compensate for the minute parasitic inductance of the chip resistor so R_{RP} would not have any reactive impedance. Total size of the fabricated 2-stage DE NGD circuit is $180 \times 90\,\text{mm}^2$.

Figure 12 shows the simulation and measurement results of the 2-stage DE NGD circuit. One notable advantage of the proposed topology is that the same magnitude and group delay response can be obtained when the position of the gain amplifier is changed. In other words, the 1st gain amplifier (G) can be moved to the output of the 2nd NGD circuit (Unit #2) according to the input power level. In that way,

we can avoid the potential nonlinear distortion generation in the NGD module. The measured results agree well with the simulation results, where the measured GD and the insertion loss were -9 ± 0.25 ns and -0.21 ± 0.06 dB in the operating frequency band, respectively. Small amount of GD and magnitude error are due to the connecting elements and the gain of the small signal amplifier. In the case that a larger negative GD would be necessary, the designer should make a trade off between the GD and the bandwidth. In regards to the additional DC power consumption in the NGDC, each small signal amplifier consists of two ERA-5SM Mini-Circuits which consume about 0.5 W.

4. EXPERIMENTAL RESULTS

The MPA of the proposed feedback amplifier was fabricated with a NPTB00025, GaN HEMT device with a peak envelope power of 25 W. The MPA_{FB} is operated by quasi class-E with a gate bias voltage of -1.9 V and driven by an MHL21336 made by Freescale. This MPA_{FB} could operate up to a 43.1 dBm of the output power (laboratory measurement) with a gain of 50 dB at 28 V. It had a 70.1% power added efficiency (PAE) at the peak output power [35]. Due to the frequency response of the employed NGDC, which also amplified the unwanted out-of-band noise, the 2-stage quarter-wavelength coupled line band-pass filter was designed with a microstrip line and integrated in the feedback loop to avoid possible instabilities. An adoption of the narrow band BPF increased the total GD of the feedback path by 2.5 ns; this factor was already considered in the previous section in the design of the NGDC.

Figure 13 shows the measured suppression characteristics of the carrier suppression loop. For the carrier bandwidth of the 2-carrier WCDMA signal, at about 10 MHz, a carrier suppression of

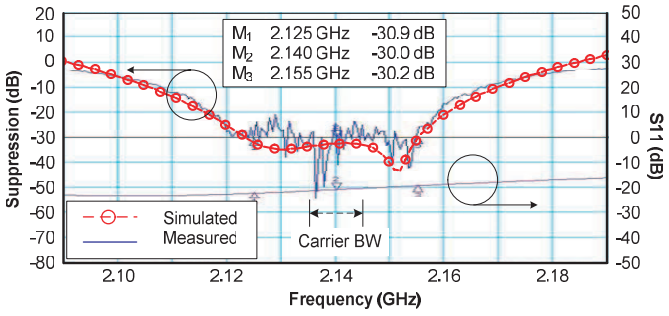

Figure 13. The measured carrier suppression loop characteristics.

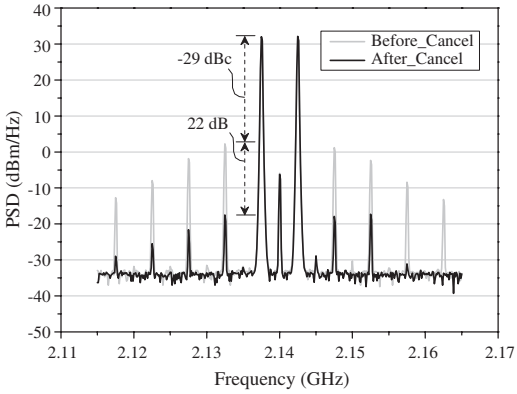

Figure 14. The measured 2-tone spectra before (Before_Cancel) and after (After_Cancel) linearization at an output power of 32 dBm/tone.

30 dB could be achieved. Considering a suppression of 20 dB as a reference, the bandwidth reaches up to around 50 MHz. Due to the feedback properties, we could not measure the IMD loop suppression characteristic. However, it was expected that a minimum IMD suppression of 20 dB would be achieved at a bandwidth of 50 MHz, based on the measured results of the carrier suppression loop.

Figure 14 shows the measured spectra of the fabricated feedback amplifier for a 2-tone signal at an output power of 32 dBm/tone. The 2-tone spacing was 5 MHz and the frequency span was 50 MHz so we could observe the IMD components up to the 9th order. Due to the gate bias condition around a deep class B, the output signal of the fabricated feedback amplifier exhibited much nonlinearity when the feedback loop was open. Over the entire bandwidth of interest, intermodulation distortion signals were suppressed by well below 20 dB after closing the feedback loop. This extremely large cancellation bandwidth is nearly 10 times the previous feedback amplifier.

Figure 15 shows the measured spectra of the feedback amplifier for a 2-carrier WCDMA signal at an average output power of 28 dBm and 33 dBm. The peak to average power ratio (PAPR) of the signal was 10.5 dB at 0.01 %. When the average output power was 28 dBm, the adjacent channel leakage ratio (ACLR) improvement was almost 25.1 dB from −26.8 dBc (Before Cancel) to −51.9 dBc (After Cancel) at a 5 MHz offset, as shown in Fig. 15(a). When the average output power was 33 dBm, the ACLR improvement was almost 23.8 dB from −24.6 dBc (Before Cancel) to −48.4 dBc (After Cancel) at a 5 MHz offset, as shown in Fig. 15(b). In the case of an output power higher than 34 dBm, the measured ACLR does not meet the linearity specification, which is −45 dBc for a base-station power amplifier.

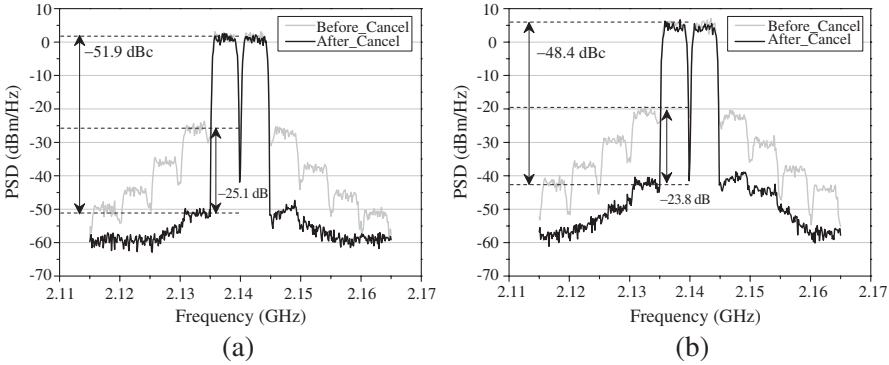

Figure 15. The measured 2-carrier WCDMA spectra (PAPR: 10.5 dB @ 0.01%) before (Before_Cancel) and after (After_Cancel) linearization at an average output power of: (a) 28 dBm, and (b) 33 dBm.

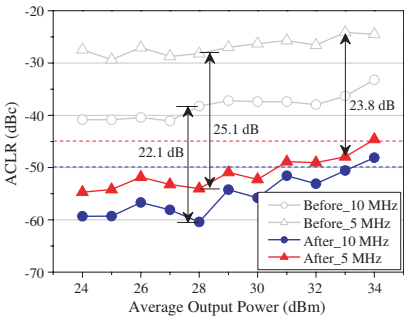

Figure 16. The measured ACLR at a 5 MHz and 10 MHz offset for a 10 dB output dynamic range before and after linearization.

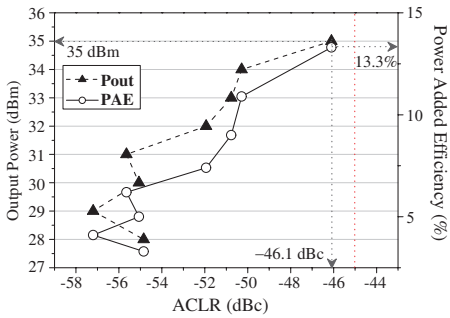

Figure 17. The measured ACLR and power added efficiency performance with respect to the average output power for a 1-carrier WCDMA signal.

Figure 16 illustrates the measured ACLR before and after linearization for a 10 dB output dynamic range using the 2-carrier WCDMA signal. Optimized for 28 dBm of the output power in terms of the linearity, the fabricated system achieved at least −45 dBc (red dotted line) of the ACLR at a 5 MHz offset for an output power between 24 dBm to 34 dBm. The maximum ACLR improvement of 25.1 dB was achieved when the output power was 28 dBm, which is a superior linearity improvement with an increased bandwidth for the feedback amplifier. It was observed that the linearity of the closed loop operation is degraded when the output power was higher than 34 dBm. The

reason is because the small signal gain amplifier used in the NGDC is thought to begin to saturate at an output power level higher than 35 dBm. Since the focus of this work is the bandwidth enhancement of the cancellation bandwidth, not the efficiency, we will not seriously discuss the efficiency issues.

The measured ACLR and PAE performance with respect to the average output power using a 1-carrier WCDMA signal is presented in Fig. 17. The proposed feedback technique achieved ACLR and PAE of −46.1 dBc and 13.3%, respectively, at an average output power of 35 dBm by using 1-carrier WCDMA signal. For the MPA without the feedback loop, the ACLR and PAE were −46.4 dBc and 2.7%, respectively, at an average output power of 26 dBm. For the same ACLR level with and without the proposed feedback topology, PAE of the system is increased from 2.7% to 13.3%. Also, considering −46.1 dBc of ACLR as a reference, the available output power for the MPA is increased from 26 dBm to 35 dBm. This efficiency included the additional power consumption of the NGDC and the other accessory feedback circuits.

The measured results and the performance comparisons among the feedback amplifiers are summarized in Table 1. Due to its extremely limited bandwidth performance, the analog feedback amplifier has not been actively studied. The 50 MHz cancellation bandwidth achieved in this work is about 10 times the previous results. This is the best result ever achieved with the analog RF feedback amplifier architecture at the time of this writing, according to the the authors' best knowledge.

Table 1. Measurement summary and performance comparison among the analog RF feedback architectures.

	Frequency (GHz)	$P_{1\,dB}$ (dBm)	Test Signal	Cancellation BW (MHz)	Linearity (dBc)	Improvement (dB)	Remarks
[16]	0.35	23	2-tone	6	−40	8	IMS'94
[17]	1.85	27	2-tone	0.5	−42	20	IMS'98
[18]	0.88	33	2-tone	6	−46	12	MWJ'05
[19]	4.00	25	2-tone	1	−40	8	IMTT'90
[20]	0.89	46	2-tone	1	−40	16	EL'95
This work	**2.14**	**43**	**2-tone**	**> 50**	**−51**	**22**	
	2.14	**43**	**WCDMA**	**> 50**	**−52**	**25**	

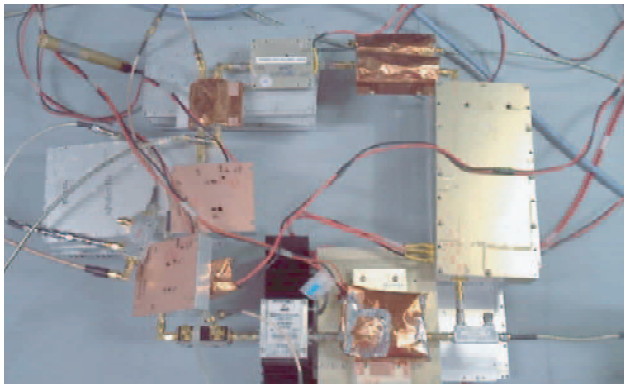

Figure 18. The photograph of the proposed analog feedback topology employing a negative group delay circuit.

A photograph of the experimental setup for the fabricated feedback amplifier configuration is illustrated in Fig. 18. In product form, all the active circuits would be integrated into one module, including the NGDC, the vector modulators, the subtractor, the BPF, and the EPA, thereby reducing the size of the whole feedback system.

5. CONCLUSION

We introduced the novel topology for analog feedback amplifiers that yields a substantial cancellation bandwidth enhancement by employing a DE NGDC. We discussed the design procedure and considerations for the DE NGDC. With the fabricated 2-stage DE NGDC for the WCDMA downlink band, the analog feedback amplifier using the proposed topology experimentally achieved the highest bandwidth among those previously reported in the literature.

Among the various linearization techniques used for base-station transmitters, although old-fashioned the analog feedback method still has many advantages over the feedforward and DPD techniques, including RF linearization, and an excellent cancellation performance compared with the linearization bandwidth methods of the feedforward structure.

REFERENCES

1. Liu, T., S. Boumaiza, and F. M. Ghannouchi, "Deembedding static nonliearities and accurately identifying and modeling memory effects in wideband RF transmitters," *IEEE Trans. Microw. Theory Tech.*, Vol. 53, No. 11, 3578–3587, Nov. 2005.
2. Black, H. S., "Translating system," U.S. Patent 1,686,792, Oct. 19, 1928.
3. Seidel, H., "A microwave feedforward experiment," *Bell Syst. Tech. J.*, Vol. 50, 2879–2916, 1971.
4. Cripps, S. C., *Advanced Techniques in RF Power Amplifier Design*, Artech House, Norwood, MA, 2006.
5. Pothecary, N., *Feedforward Linear Power Amplifiers*, 125–138, Artech House, 1999.
6. Kenington, P. B., *High-linearity RF Amplifier Design*, Artech House, 2000.
7. Hau, Y. K. G., V. Postoyalko, and J. R. Richardson, "Sensitivity of distortion cancellation in feedforward amplifiers to loops imbalances," *IEEE MTT-S Int. Microwave Symp. Dig.*, 1695–1698, 1997.
8. Kang, S. G., I. K. Lee, and K. S. Yoo, "Analysis and design of feedforward power amplifier," *IEEE MTT-S Int. Microwave Symp. Dig.*, 1519–1522, 1997.
9. Konstantinou, K. and D. K. Paul, "Analysis and design of broadband, high efficiency feedforward amplifiers," *IEEE MTT-S Int. Microwave Symp. Dig.*, 867–870, 1996.
10. Andrenko, A. S., K. Horiguchi, M. Nakayama, Y. Ikeda, and O. Ishida, "Optimization analysis of feedforward power amplifier," *IEEE MTT-S Int. Microwave Symp. Dig.*, 626–629, 1999.
11. Jeong, Y., D. Ahn, C. D. Kim, and I. Chang, "Feedforward amplifier using equal group- delay signal canceller," *IEEE MTT-S Int. Microwave Symp. Dig.*, 1530–1533, 2006.
12. Choi, H., Y. Jeong, J. S. Kenney, and C. D. Kim, "Dual-band feedforward linear power amplifier for digital cellular and IMT-2000 base-station," *Microw. Optical Technol. Lett.*, Vol. 51, No. 4, Apr. 2009.
13. Choi, H., Y. Jeong, J. S. Kenney, and C. D. Kim, "Cross cancellation technique employing an error amplifier," *IEEE Microw. Wireless Compon. Lett.*, Vol. 18, No. 7, 488–490, Jul. 2008.
14. Seidel, H. and N. J. Warren, "Reentrant signal feedback

amplifier," U.S. Patent 3,624,532, Nov. 30, 1971.

15. Seidel, H. and N. J. Warren, "Feedback amplifier," U.S. Patent 3,656,831, Apr. 18, 1972.
16. McRory, J. G. and R. H. Johnston, "An RF amplifier for low intermodulation distortion," *IEEE MTT-S Int. Microwave Symp. Dig.*, 1741–1744, 1994.
17. Kim, Y., Y. Yang, S. Kang, and B. Kim, "Linearization of 1.85 GHz amplifier using feedback predistortion loop," *IEEE MTT-S Int. Microwave Symp. Dig.*, 1675–1678, 1998.
18. Qiang, L., Z. Z. Ying, and G. Wei, "Design of a feedback predistortion linear power amplifier," *Microwave J.*, Vol. 48, No. 5, 232–241, May 2005.
19. Ezzeddine, A. K., H. Hung, and H. Huang, "An MMAC C-band FET feedback power amplifier," *IEEE Trans. Microw. Theory Tech.*, Vol. 38, No. 4, 350–357, Apr. 1990.
20. Faulkner, M., D. contos, and M. Johansson, "Linearisation of power amplifiers using RF feedback," *Electronics Lett.*, Vol. 31, No. 23, 2023–2024, Nov. 1995.
21. Solli, D. and R. Y. Chiao, "Superluminal effects and negative group delays in electronics, and their applications," *Physical Review E*, Vol. 66, No. 5, 056601.1–056601.4, Nov. 2002.
22. Brillouin, L. and A. Sommerfeld, *Wave Propagation and Group Velocity,* 113–137, Academic Press, Network, 1960.
23. Lucyszyn, S., I. D. Robertson, and A. H. Aghvami, "Negative group delay synthesizer," *IEE Electron. Lett.*, Vol. 29, No. 9, 798–800, Apr. 1993.
24. Wang, L. J., A. Kuzmich, and A. Dogariu, "Gain-assisted superluminal light propagation," *Nature*, Vol. 406, No. 6793, 277–279, Jun. 2000.
25. Kitano, M., T. Nakanishi, and K. Sugiyama, "Negative group delay and superluminal propagation: An electronic circuit approach," *IEEE Journal of Selected Topics in Quantum Electronics*, Vol. 9, No. 1, 43–51, Jan. 2003.
26. Noto, H., K. Yamauchi, M. Nakayama, and Y. Isota, "Negative group delay circuit for feed-forward amplifier," *IEEE Int. Microwave Symp. Dig.*, 1103–1106, 2007.
27. Ravelo, B., A. Perennec, and M. Le Roy, "Synthesis of broadband negative group delay active circuits," *IEEE Int. Microwave Symp. Dig.*, 2177–2180, 2007.
28. Ravelo, B., A. Perennec, M. Le Roy, and Y. Boucher, "Active microwave circuit with negative group delay," *IEEE Microw.*

Wireless Compon. Lett., Vol. 17, No. 12, 861–863, Dec. 2007.

29. Ravelo, B., A. Perennec, and M. Le Roy, "Negative group delay active topologies respectively dedicated to microwave frequencies and baseband signals," *Journal of EuMA*, Vol. 4, 124–130, Jun. 2008.
30. Ravelo, B., M. Le Roy, and A. Perennec, "Application of negative group delay active circuits to the design of broadband and constant phase shifters," *Microw. Optical Technol. Lett.*, Vol. 50, No. 12, 3078–3080, Dec. 2008.
31. Choi, H., K. Song, C. D. Kim, and Y. Jeong, "Synthesis of negative group delay time circuit," *Asia-Pacific Microwave Conf. Dig.*, B5–08, 2008.
32. Choi, H., S. Shim, Y. Jeong, and C. D. Kim, "Synthesis of reflection type negative group delay circuit using transmission line resonator," *Proc. 39th European Microwave Conf.*, 902–905, Sep. 2009.
33. Jeong, Y., H. Choi, and C. D. Kim, "Experimental verification for time advancement of negative group delay circuit in RF electronic circuits," *IET Electron. Lett.*, Vol. 46, No. 4, 306–307, Feb. 2010.
34. Matthaei, G., L. Young, and E. M. T. Jones, *Microwave Filters, Impedance-matching Networks, and Coupling Structures*, Artech House, Dedham, MA, 1980.
35. Choi, H., Y. Kim, Y. Jeong, J. Lim, and C. D. Kim, "A compact DGS load-network for highly efficient class-E power amplifier," *Proc. 39th European Microwave Conf.*, 1353–1356, Sep. 2009.